Albinoni Analysis Status

DRAFT V4
July 20, 2004

V. Fadeyev, G. Aldering, R. Thomas

Abstract: **We describe the analysis of SN1998eq (Albinoni), a SN of redshift 1.2 . Photometric measurements were performed on both the I-band ground-based data, and HST data. The latter includes both the I-band data taken with WFPC2 and J-band data taken with NICMOS. The photometric procedures account for the presence of significant host galaxy light contamination. The data were color-corrected to the I-band lightcurve, which was subsequently fit to extract the restframe U-band stretch and maximum (m(U)). A first estimate of the extinction was obtained by comparison of the I-band lightcurve and NICMOS J-band photometry point. This resulted in preliminary E(B-V) value of 0.075 +- 0.080. We translated m(U) to m(B) and added the high-redshift point to the sample of Knop et al 2003[1]. Remaining work includes refinement of the K-correction and extinction estimate using the ground-based Keck spectrum.**

Table of Contents

1. Introduction

The high-redshift supernova, code-named Albinoni, was discovered in the Keck search run in fall of 1998. The host-galaxy [OII] emission line in the spectrum, taken near maximum, gave an accurate redshift of 1.2, and the spectral shape was a good match to a Type Ia SN. Pre-scheduled HST observations were obtained at several epochs in F814W and a single epoch of F110W. Subsequent analysis [2] revealed that SN is positioned on top of its host, which due to the high redshift, is small in angular

size. The host contamination necessitated taking final references exposures. Unfortunately, the NICMOS instrument became inoperative at the end of 1998 due to premature depletion of the coolant [3]. Not until March 2002 was the instrument revived, by installing a mechanical cooler. The final references were obtained in fall of 2002, at which point the collaboration was in a position to analyze the data.

The available data sample is presented in Table 1.

Table 1 Summary of Albinoni Dataset.

Dataset	***N epochs***	***Time [Ksec]***	***Obs. Dates in '98***	***Comments***
Keck LRIS I-band images	4	2-8	9/15, 10/15, 11/03, 11/04	Calnights 9/15, 10/15, 11/04
HST WFPC2 I-band images (F814W)	4	1.5-7.5	10/26, 11/09, 11/19, 11/30	
HST NICMOS J-band images (F110W)	1	10.3	11/18	
Keck LRIS spectrum				
Final References				
Keck LRIS I-band images	1	3.6	10/13/99	
ESI I-band images	1	1.2	11/10/02	
HST WFPC2 I-band images (F814W)	1	16.1	07/20/01	
HST NICMOS J-band images (F110W)	1	8.1	12/09/02	

The rest of this note is organized as follows. The photometric processing and cross-checks are described in Section 2, the lightcurve fit is shown in Section 3, the extinction estimate is given in Section 4, the cosmological results are given in Section 5, and conclusions are presented in Section 6.

2. Photometry

1. Ground-based photometry of Keck LRIS data

Due to computer disk failures at LBL the files from original data reduction were not fully available. We recovered the raw data from Exabyte tapes and re-reduced

them. The reduction followed the prescriptions in Rob's manual [4]. The basic steps are bias subtraction, trimming, gain multiplication, zero-readout frame subtraction, flatfielding and fringe subtraction.

Whenever possible we tried to make a flatfield from night-sky observations. For the nights of November 3 and 4 the sky exhibited large variable gradients across the field, up to 9 % across the image, possibly due to the bright moonlight on those nights. For these nights, we made the flatfields from dome flats, and subsequently subtracted the fringes according to the airmass and exposure time. The fringe removal was not done for the nights of September 15 and October 15, because the flatfield made from night-sky observation contains the fringes, and division by the flatfield greatly reduces them. Further attempts to subtract fringes did not improve the scatter of the sky pixels. Attempts to make a flatfield from twilight observations were not successful, due to the limited number of exposures and the presence of stars in most images. As the result of the reduction, the sky RMS became close to the expected Poisson variance. Typical numbers are: sky level of 65000 e^- (which implies noise of 255 e^-), sky RMS of 300 e^-. Flatfielding errors of a few-tenths of a percent would be sufficient to explain the excess noise.

As shown in Table 1, for 3 out of 4 Keck observation nights we had Landolt stars calibration data. We ran the standard SCP procedure ***photocalib*** to extract the zeropoints (ZP), airmass term (AM) and color term (CL) from these data. The ***calibnights*** file, which is the SCP photometric database, was updated. For one of the nights, September 15, we got the same result as Rob got previously. For the other two nights, the entries are new. For the night of October 15 we were able to solve for ZP, AM and CL. The available range of airmasses for the Landolt stars observation did not allow a solution for AM for the night of November 3. Neither AM nor CL could be extracted for the night of September 15. Guesses (standard telescope values) were substituted for the AM/CL terms when they could not be extracted with calibration procedure. As of the time of this note, all three calibration nights are chosen, including the guesstimates. As a future step, we should limit ourselves to the only night with complete zeropoint assessment.

The photometric processing of the Keck data was done with SCP standard software suite ***ivanlight*** [5]. We iterated on the SN position 4 times to make sure that the SN aperture was correctly centered [6].

2. HST WFPC2/PC photometry

We obtained the reduced WFPC2 data from STSCI archive, and selected PC camera images for further processing. All SN images were targeted with PC, since it features the smallest pixel scale of 0.046". We used the standard ***crrej*** procedure to clean them of cosmic rays. The procedure is a part of IRAF package ***stsdas.hst_calib.wfpc*** . It works by comparing the pixel values in the input images, assuming but very small relative shifts, and removing the positive outliers. The output is a single image “stack”.

The assumption of positional matching of the input frames works well for exposures taking in the same orbit. HST pointing stability from orbit to orbit is much worse, with shifts on the order of 1 PC pixel size. Correspondingly, we grouped the images on the per-orbit basis for the cosmic ray removal and further processing. For

two epochs, a region near the SN was completely zapped by a CR in one of the exposures. Such image was removed from the processing. (The other image from the same orbit was retained in each case.)

The Albinoni final reference data consist of 6 one-orbit dithered exposures. Therefore, the ***crrej*** procedure was not applicable. To obtain the combined image, and remove CRs we used the ***drizzle*** procedure [7]. The relative shifts between images obtained from the image headers were different from the ones obtained from the jitter files. This inconsistency required us to hand-tune the shifts based on an unsaturated field star in the PC image.

The SN image on November 9 is shown in Figure 1, and the combined final reference image is shown in Figure 2. It is obvious that the host galaxy has a small size, which represents a fast spatially-variable background for SN measurement. For this reason, the method of approximating the host galaxy light by low-order polynomial functions, as was done in Rob's paper [1], is not adequate in this case.

We extended Rob's HST software [7] to include additional galaxy parameterizations:

1) Exponentially decaying ellipsoid, $Flux = A * \exp(-R/R_0)/R_0^2/a/(1-a)$, where $R = \sqrt{(x'/a)^2 + (y'/(1-a))^2}$, and $x' = (x-x_0)*\cos(\alpha) + (y-y_0)*\sin(\alpha)$, $y' = (y-y_0)*\cos(\alpha) - (x-x_0)*\sin(\alpha)$. This parameterization has 6 parameters: flux normalization A, decay constant R_0, ellipticity a, rotation angle α, and position x_0, y_0.
2) Gaussian ellipsoid, $Flux = A * \exp(-R^2/R_0^2/2)/R_0^2/a/(1-a)$ with similar parameters definition. Such a parameterization is not expected to properly model a real galaxy.

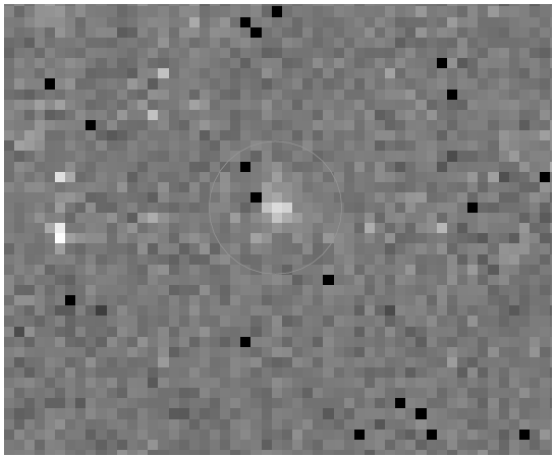

Figure 1. Combined SN image on November 9. The position of SN and its host galaxy is indicated by the circle. The pixels with bad data quality flag are shown in black. The non-SN white pixels have residual CR effect. The exposure time is 2.7 Ksec. The "Z-scale" parameters are z1=-12, z2=22.

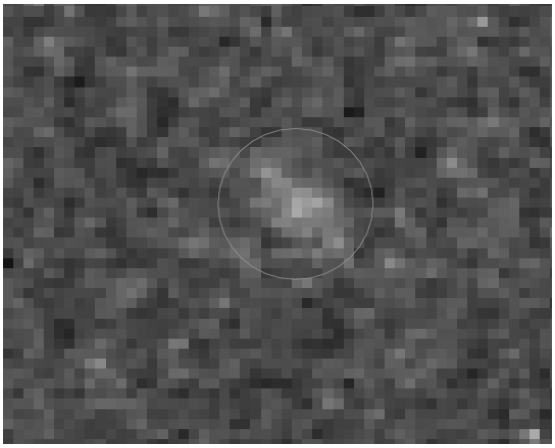

Figure 2. The drizzled final reference image with the same orientation as in Figure 1. The circle indicates the host galaxy position. The exposure time is 16.1 Ksec. The "Z-scale" parameters are z1=2, z2=7.

We chose to have two different background parameterization functions in order to assess the sensitivity of our result to the background modeling.

In each case, the numerical parameters were found by fitting the background shape to the final reference image. Then the shape was inserted into the HST software, with fixed R_0, a, α. The software was fitting for the SN flux and position for a given epoch, as well as the global fit parameters: host galaxy flux normalization A, and relative SN/galaxy position.

We decided to let the fit determine the host galaxy flux due to the galaxy faintness and associated CTE effect. The ratio of the galaxy flux returned by the HST fitting software to the value from the final reference fit is (1.01 ± 0.17). This result is consistent with the CTE effect not changing by a large amount in the presence of the SN.

The usual CTE parameterization [9] is only valid for stars, and not applicable for the extended objects. We made a rough estimate of the *absolute* value for the final reference CTE by considering the central 4x3 galaxy pixels. It turns out to be (21 ± 2) % effect. Note however, that the galaxy halo may invalidate the star PSF assumption that went into the parameterization.

We also attempted to estimate the CTE by comparing the WFPC2 final reference galaxy flux measurement with the one from the ground. The results differ for different galaxy parameterizations. For the exponential one, we get FluxWFPC2/FluxLRIS = (1.29 ± 0.23). For the Gaussian case, we get FluxWFPC2/FluxLRIS = (1.04 ± 0.21). One would expect that the ratio would be less than one, because the ground data do not suffer from the CTE effect. However, due to the large errors, this measurement is inconclusive, and may be consistent with the parametric CTE estimate above.

Note that the software fit was assessing the *relative* CTE difference between the final reference and the SN explosion time. There are three effects that influence the result:

- The continuing degradation of the CCD with time.
- The different background levels for the follow up and final reference images. The

latter exposures are about factor of 2 longer.

- The PC readout direction is downward, therefore the SN is in front of a part of the galaxy.

The parameterized galaxy core estimate indicates that the combined effect of the time and exposure depth is to make the galaxy amplitude 7+-3 % higher in the final reference image. The galaxy screening by the SN should produce the opposite effect, which is hard to quantify.

The CTE effect on the lightcurve is described in section 3.

The fit returns the relative separation between the SN and the host galaxy of (1.71 ± 0.45) pixels, which corresponds to (0.078 ± 0.020) ".

The other aspects of the photometric processing are based on the standard framework, featuring CTE parameterization and Vega zeropoints from Dolphin [9], as well as the TinyTIM psf model [10].

As an illustration of the output, we give the photometric yield for the four epochs in Table 2. Note that this is somewhat incomplete information, since the measurements at different epochs are correlated via the common background model. The correlation coefficients vary from 7 to 11 %.

Table 2. Albinoni flux in WFPC2/PC with F814W filter.

Epoch	**Average flux in F814W [e^-/sec]**
October 26 '98	0.497 ± 0.065
November 9 '98	0.339 ± 0.036
November 19 '98	0.239 ± 0.020
November 30 '98	0.141 ± 0.022

We performed the following crosschecks to ascertain the validity of the results:

1) Fits with alternative parameterizations. The Gaussian parameterization gives 1 to 2% higher yield than the exponential one, depending on the epoch.
2) Varying TinyTIM PSF models. The HST fitting software framework assumes a single PSF model for all the lightcurve epochs. The variation of the SN spectrum with epoch affects the PSF width to a degree dependent on the filter width. We ran the fits with different spectral models for different epochs to find out the size of the effect in our case. The output fluxes varied by 3 % in the most extreme case. Most fluxes fluctuated by 1-2 %.
3) Alternative ***crrej*** processing. To verify that the crrej procedure did not introduce a significant bias, we varied the processing parameters: ***scalenoise*** and thresholds. The photometric yield was stable, with maximum deviation of $0.2\,\sigma$ in the worst case.

We conclude that the results are stable, and that the aspects of the processing that we studied do not introduce a noticeable significant bias.

3. Crosscheck with ground-based data.

Given the differences in software processing and the calibration procedure between the ground-based and space data, it would be prudent to crosscheck the relative photometric output. Since the PC camera has a small field of view of 34x34", our HST observations do not contain many objects. We used the only non-saturated field star available to do the crosscheck. Figure 3 gives the star lightcurve, normalized to WFPC2/PC flux in [e^-/sec]. The Poisson error for the ground-based observations is small enough that other effects, such as flatfielding errors, likely dominate the total uncertainty. The photometry for each epoch was derived from the individual exposure fluxes by averaging them. The associated error was assessed as .

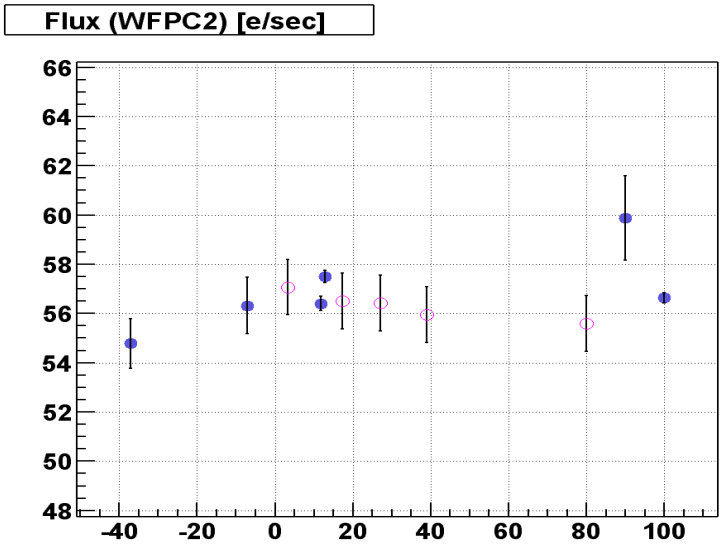

Figure 3. Field star lightcurve. The horizontal axis is the time relative to the Albinoni maximum [day]. The last three measurements to the right are from the final references images. Their timing is offset from the true one by several hundred days. The blue filled circles are from the ground measurements. The red open circles are from the HST observations; we assumed a 2% photometric error for all of them. The scatter of the HST points is less than the error. There may be a common correlated error component for the HST observation.

As shown in the plot, the ground- and space-based photometry results match within 2% or so. We regard this as an excellent correspondence, indicating no sizable systematic bias. Note that, as will be shown in the previous section, our SN photometry errors are 10% or larger.

4. NICMOS photometry.

NICMOS data feature many artifacts [11], and some amount of handwork is necessary to produce quality results. The pipeline output images suffer from spurious bias jumps in different quadrants, resulting in different background levels. The

standard recommendation is to reprocess the data including the ***pedsky*** procedure to reduce this bias error.

In addition to known NICMOS features, we noticed three additional features:

1) there are positive outliers near the location of large CR energy deposition (the CR spike itself is removed by the pipeline processing),
2) the error array associated with the count rate measurement does not reflect the count spread for the sky pixels,
3) there are pixels with consistently high or low values in different images,
4) there was a large gradient along the X-axis of the images for the data taken in 1998.

Note that most of the features may not be a problem for many other observations. Our task is to make an accurate measurement of a faint signal, therefore the similar size image artifacts are worth considering.

To fix problems (1) and (2), we modified the pipeline software. The exact details are a subject of another write-up [12]. In short, there are three areas of improvements:

- Improved CR jumps treatment. In the official version of the software the CR-induced jumps in the readouts were handled by downshifting the post-jump values. The amount of the shift was calculated from the two adjacent readouts in the jump region. Such calculation incurs the error due to the readout noise, and can therefore offset the remaining post-jump readout values. We handle such cases by joint linear fits in the pre- and post- jump regions. The fits are constrained to have a common slope (count rate). They naturally have different intercepts.
- We find that the edge neighbors of the pixels with CR jumps can exhibit moderate jumps at the same readout time. In such cases the jump can be below the threshold to pass the CR trigger, but high enough to affect the count rate determination, when measuring faint sources. Therefore, we applied the CR rejection procedure to the edge neighbors of the pixels with identified CR jumps. (The corner neighbors do not show correlated jumps, and therefore are not affected.) This procedure represents a departure from the strictly per-pixel data processing at this stage of calibration.
- The errors derived from the linear fits to the readout values do not represent the true spread of the derived count rate. The scale of the mismatch increased with the rate. This is due to the correlations between readout values. (The implemented linear fit assumes uncorrelated data.) We re-derived the errors to account for the correlations. The new errors are within about 10% of the true count rate spread. Therefore, they can now be used in photometry (and drizzling) alongside with the count rates themselves.

To fix problem 3, we made our own custom bad pixel maps on the basis of other scientific observations taken at about the same time. The basic idea is to find pixels that are consistently high/low in many images. The high/low criterion is defined wrt the neighboring pixels. The following steps undertaken to make the maps:

- First, a set of “many” images (at least 20 or so) close in time to the target observation was chosen. They were required to be mostly empty (no large extended objects), and not have a noticeable post-SAA glow. The Albinoni images were not included in making the map.
- Then for each pixel of each image a nearest 11 by 11 "patch" around that pixel is

chosen, so that it fits in the pixel's quadrant. I.e. if a pixel is someplace in the middle of the quadrant, then the patch is centered on the pixel. If the pixel is close to the edge of the quadrant, then the patch "touches" the edge, but stays inside the quadrant. This condition of "staying inside" is meant to avoid potential problems due to imperfect bias equalization.

- "Bad" pixels, including the ones with flag of 1024 (sources) are vetoed. The rest are used to do a 2D linear function fit in the patch. The fit is iterative. The residuals are histogrammed, and the histogram is used to infer the global pixel error for the patch. The pixels that are more than 3 standard deviations away from the function are vetoed, and the fit is reiterated until stable. The result of the fit is the deviation (in sigmas) between the pixel value and the fit function from the corresponding patch.
- The pixels that were at least 5 standard deviation positive/negative outliers in at least half of the images, in which they were not flagged as "sources", were considered to be consistently warm/cool. The combination of warm and cool pixels was used to make a map that was added to the default "official" one.

Problem 4 is caused by an anomaly peculiar to the readout scheme used for the data take in 1998. In that scheme, there were multiple readouts at the end of exposure designed to minimize the error on the derived count rate. Unfortunately, the readout electronics temperature is higher in the case of fast readouts. When the temperature is stable, the effect on the imaging is minimal. However, when the temperature is changing, as is the case for the first fast readout at the end of the sequence, the sky appears to have a gradient in the direction of the slow readout (X-direction for camera 2). Examination of the individual readout frames revealed that other readouts do not exhibit this feature. Ideally, one could take care of this issue by constructing a special “dark” frame for this readout and further modifying the pipeline software. Since only one of the 25 readout frames was affected, we opted for vetoing the problematic readout from the sequence.

The final reference images presented an additional “known” problem of the South Atlantic Anomaly. When HST passes through the SAA region in the sky, numerous cosmic rays bombard it. Scientific operations stop during the passage, and this circumstance is not a problem for most instruments. The NICMOS imager, however, suffers a substantially elevated dark current level in the locations where CRs have passed. This dark current decays in the course of 1-2 hours. The exposures taken immediately after the passage are affected. They have a “blotchy” look. This phenomenon was not anticipated, and some NICMOS exposures of other SNe taken by the SCP early in 1998 were rendered unusable due to this affect. The Albinoni signal observations were not affected, however the final references, taken after the re-start of the NICMOS operations, are. By that time, a special procedure was developed to provide information about the affected pixel locations. Two 10-minute special exposures (“darks”) are taken immediately after each SAA passage. An analysis of the subsequent scientific exposure can, in principle, take advantage of this information. Presently, there is a recommended IDL code, which uses the post-SAA darks to minimize the noise in the affected pixels for the subsequent scientific exposure. At the time of our analysis, this code was not yet available, and we took a more conservative route. Each of the post-SAA darks is processed in the fashion similar to the bad pixel

identification algorithm outlined above. Then a $\chi^2=((dev_1/sigma_1)^2+(dev_2/sigma_2)^2)/2$ is constructed for every pixel on the basis of the two exposures. A cut of $\chi^2 > 1.5$ is imposed to make a map of the affected pixels. (Only pixels having positive deviations in both images are considered.) The map is then used to veto the bad pixels from the rest of the processing.

The net result of the processing is images with a high degree of sky uniformity, with reliable associated error estimates and bad pixels flagged.

We do the photometric processing with custom software routines based on ROOT [13]. The software was written with NICMOS data in mind, incorporating the bad pixel maps and the count rate error array. The TinyTIM psf fitting and the galaxy background model are included. (These aspects differentiate the procedure from the previous analysis [14].) The χ^2 minimization step is based on MINUIT framework [15] included in ROOT. The underlying concept for the fitting is similar to that of the HST software [7], and the existence of these two similar PSF fitting methods is due to historical reasons. Note that, unlike the CCD-based devices, the infrared arrays do not have issues with CTE corrections or inter-pixel diffusion.

We crosschecked the performance of our software routines on HST standard stars images. Solar analogs P330E, P177D, and white dwarfs G191B2B and GD153 were NICMOS photometric standards, and their images were available in the archive. For cases with stars away from the bad regions (central bad column etc) we performed both the aperture photometry and our PSF-fitting. The results matched within 1.5% accuracy.

Since later on we are going to compare the NICMOS photometry with Vega-calibrated WFPC and Keck data, we contrasted the NICMOS photometry with the available normalized spectra of the standard stars. The photometric fluxes turn out to be less than the projected values on the basis of the spectra. The average effect is 3.5% for the four standards. Attempts to attribute the effect to errors (shifts in wavelength or a slope with wavelength across the filter curve) in the official HST throughput curve were not successful. “Tilting” the throughput curve would require relative correction of 0.6 (0.1) for the ends of the passband for the solar analogs (white dwarfs). “Shifting” the throughput curve would require 470 (90) A change for the solar analogs (white dwarfs). Therefore, the effect should be related to overall throughput scale. We will correct the SN photometric yield by the size of the effect.

We generated the TinyTIM model, to be used in the fit, based on Rob's “uberspectrum” model and the timing of the NICMOS observation relative to the lightcurve.

The galaxy shape was parameterized with a function similar to that used for the WFPC2 data. The relative SN/galaxy position was taken from the WFPC2 fit and fixed during the fit. The positional accuracy derived from the WFPC2 fit was factor of 2 better than the stand-alone NICMOS evaluation. The latter suffered from the small field of view, and, as a consequence, an absence of bright alignment objects in the images.

There was a temperature change between the initial NICMOS operations and its use after the revival. We scaled the final reference galaxy flux based on the photometric calibration for the two epochs.

Figure 4 shows the SN photometric yield as a function of the exposure number.

We do not see any obvious systematic trend in this plot, except that every 3rd observation has larger error due to shorter exposure time.

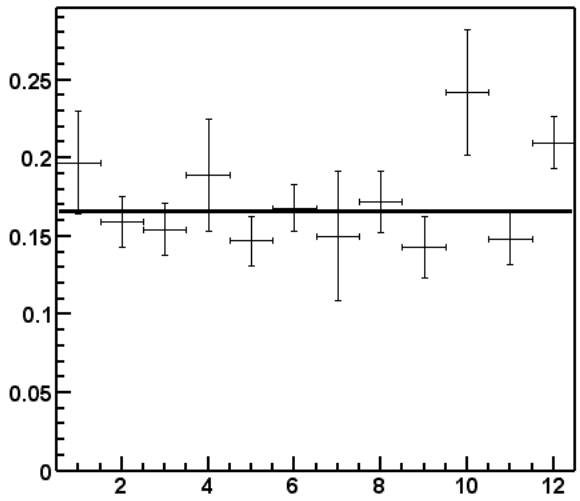

Figure 4. Albinoni photometric yield [counts/sec] in NIMOS J-band as a function of exposure number.

The derived flux is (0.1663 ± 0.0057) cnt/sec, and χ^2/N(DoF) = 1.51. As a crosscheck, we also made the drizzled images of the SN follow-up and the final reference, and subtracted them to obtain a SN-only image. Fitting a TinyTIM model revealed that the SN image is substantially wider than the model PSF. This could be due to positional shifts between different exposures. We incorporated 2D Gaussian smearing into the fitting procedure to match the SN shape. The flux thus obtained is (0.1738 ± 0.0040) cnt/sec.

We correct the raw flux measurement for the large-angle flux (i.e. the flux outside of our 3" TinyTIM model), by the factor of 1.030, and also by the throughput factor of 1.034. The net result is (0.178 ± 0.006) cnt/sec.

The following are the systematic effects we have considered. In each case a parameter or a procedure was varied, the fit was reiterated, and the resulting difference in the extracted flux was treated as the error estimate.

- Relative SN/galaxy position. We varied the position estimate from WFPC2/PC fit by its error and reiterated the fit. This is 2.0% effect.
- Galaxy flux uncertainty. We varied the galaxy parameterization flux by its error and reiterated the fit. This is 2.6% effect.
- Galaxy shape error. We compared the results with exponential and Gaussian background shape parameterizations. The difference is small, 0.4%.
- TinyTIM shape modeling. We varied the field position, PAM variation, cold mask wiggle, and timing of the SN spectrum in the model generation. The fit was reiterated each time to assess the effect on the photometry. The net effect is 1.5%, with the larges contribution being the field position of the SN (1.2%).
- We varied the SAA rejection algorithm threshold. The effect is 1.5%.
- We varied the CR rejection threshold in the pipeline processing. The effect is 1.9%.
- There is a diffraction spike from a nearby bright star (the star itself is outside of the field in most exposures, but the diffraction spike shows up in the images, passing

near the SN position). We removed a part of the fitting area containing the ray from the fit. This made a 0.4% difference.

- There is an official number for the photometric scale accuracy of 2.0%.

We consider most of the systematic effect to be uncorrelated. A notable exception is the photometric scale accuracy possibly being correlated with SN position in the PSF shape modeling. We add the systematic errors in quadrature to obtain the aggregate error of 4.8%. Note that the MINUIT fit was not marginalized over the input parameters, and the presented assessment of the flux variation for 1-σ parameter change is the adopted way of propagating the errors. We scale the 3.4% error from the fit by the χ^2/N(DoF) value to get the fit error of 5.0%. The combination of systematics and the fit error gives 6.9% accuracy.

3. Lightcurve fit

As shown in Figure 5, the LRIS I-band, Bessel I-band and F814W are substantially different. We follow the prescription of Knop '03 [1] of color-correcting the LRIS and HST data to the same system (Bessel I-band) in order to make a complete lightcurve. The color corrections are about 0.09-0.19 mag for LRIS and -0.07 mag for HST.

The observer I-band at redshift of 1.2 is well matched by the restframe U-band. We use the corresponding k-corrections in order to fit the lightcurve. Both the color and the k-corrections are derived in two ways: a) from the Rob's uberspectrum at the time of the paper [1], b) from Rollin's upcoming SCP-standard k-correction machinery. The latter derivation is based on the Peter's newly tuned uberspectrum.

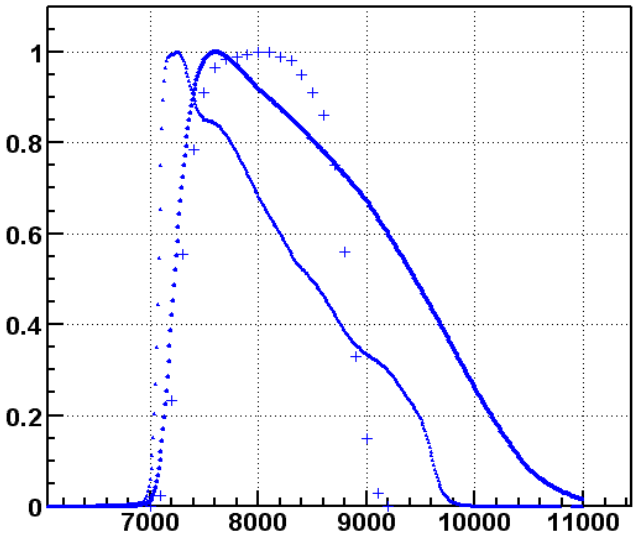

Figure 5. The I-band-like passbands: 1) HST F814W, peaking at 7200A, 2) LRIS I-band, peaking at 7600A, 3) Bessel I-band, peaking at 8000A.

We fit the lightcurves for both derivations of the color and k-corrections (Figures 6,7, Table 3).

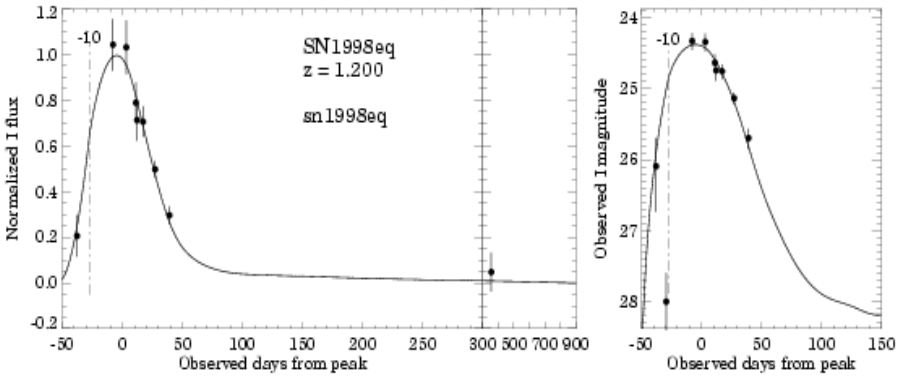

Figure 6. The I-band lightcurve fit. The color and k-corrections are derived from Knop '03 uberspectrum. The 2nd final reference measurement from the left plot is plotted on the right plot, since it is beyond the axis limits.

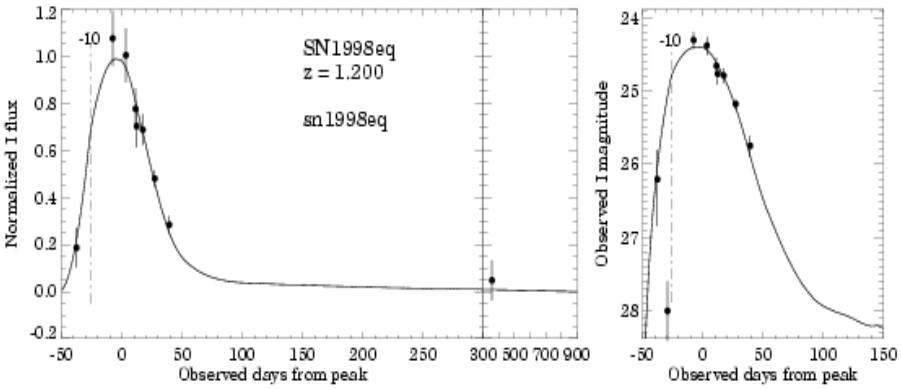

Figure 7. The I-band lightcurve fit. The color and k-corrections are derived from new Peter's uberspectrum. The 2nd final reference measurement from the left plot is plotted on the right plot, since it is beyond the axis limits.

Table 3. The lightcurve fit results.

Uberspectrum	***Tmax***	***Stretch***	***M(U)***	***M(Ucorr)***	χ^2***/#DoF***
Knop '03	51109.5 +- 2.1	1.24 +- 0.07	25.01 +- 0.10	25.36 +- 0.17	85.10/96
Nugent '04	51109.4 +- 1.9	1.20 +- 0.07	25.00 +- 0.09	25.30 +- 0.17	85.88/96

As a check, we varied the host galaxy amplitude obtained in the WFPC2 fit by 1 sigma upwards. This changes the SN flux by 2-10% depending on the epoch. The corresponding change of parameters is small; for example, the stretch value is reduced by 0.02.

The SN extinction affects the lightcurve estimate via the assumed spectral

model in the k-correction formalism. So far in this analysis we have accounted for the Galactic extinction of E(B-V) = 0.042, but have not treated the host galaxy extinction. To assess the sensitivity of the results to the assumed extinction, we repeated the fit assuming $E(B-V)_{host} = 0.2$. The stretch changed by 0.01. This shows that the extinction is unlikely to affect the lightcurve substantially. However, for completeness we will reiterate the fits after the extinction estimate.

4. Extinction estimate

1. Photometric estimate formalism

To estimate the extinction, we took the I-band lightcurve value at the time of NICMOS observation, and estimated a possible NICMOS yield on the basis of the spectral model and assumed extinction.

$$Count_{F110W} = \frac{Area}{hc * gain} * \frac{Count_I}{10^{ZP/2.5}} * \int \lambda S_{Vega}(\lambda) I(\lambda) d\lambda * \frac{\int \lambda S_{SN}(\lambda, A, t_{NIC}) J(\lambda) d\lambda}{\int \lambda S_{SN}(\lambda, A, t_{NIC}) I(\lambda) d\lambda}$$

Due to the significant width of the NICMOS filters, the observed magnitude is likely to be a function of the assumed spectrum. Therefore, we do not transfer the NICMOS counts into a J magnitude. Instead, the I-band magnitude is converted into flux units, and the two fluxes are compared based on the uberspectrum model.

At present, only Knop '03 uberspectrum is used for this purpose. The corresponding software development for the new SCP framework is pending.

The I-band measurement at the time of the NICMOS observation is estimated from the lightcurve parameters, including the correlations. Imag = 25.09 +- 0.07.

2. The input color

The proper SN color is a crucial input to the extinction estimate. In our Knop'03 paper a color of U-B = -0.4 was used, and was taken to be constant over the small range of stretches observed for the few SNe which were analyzed using restframe U-band data. In our case, the stretch value is fairly large, s=1.2, and we need to assess the appropriate U-B color to use in this case.

To estimate the color as a function of stretch, we looked at Jha's thesis data [16]. That work features the un-reddened U-B color as a function of V-band stretch (Figure 3.10). We re-plotted the data as a function of the U-band stretch, as shown in Figure 8. The data are fit to the exponential function, plateauing at high stretches. We use method from reference [17] to fit the data with the errors in both X and Y dimensions. The quality of the data is not sufficient to exclude other obvious parameterizations (linear, quadratic, etc). However, the data of un-reddened B-V color as a function of stretch is fit well by the same function, but not others (Figure 9). This forms the justification for considering only the exponential model. Two extreme color outliers were removed from both Figure 8 and Figure 9. For s=1.2 we estimate U-B (max) = -0.70 +- 0.02 assuming the exponential model is adequate.

We should note that the lightcurve parameterizations by Jha differed from Knop '03. Jha parameterized U/B/V templates on the basis of SN1998aq alone, and

then normalized his lightcurve templates to stretch=1 case by fitting his B template to a previous SCP publication [18]. Rob proceeded instead by using multiple nearby SNe to construct a template in each band with a spline under tension. Five previously published SNe were used for the Knop '03 U-band template, and data from Hamuy and Riess were used for the B and V templates. One could expect some, presumably small, differences in the definition of stretch as given by Jha compared to the stretch given by Knop '03 due to these two varying approaches.

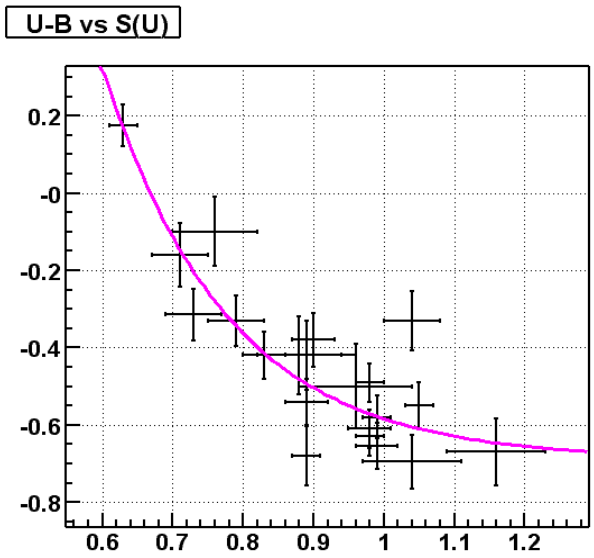

Figure 8. U-B intrinsic color at maximum versus the U-band stretch, fit to an exponential function.

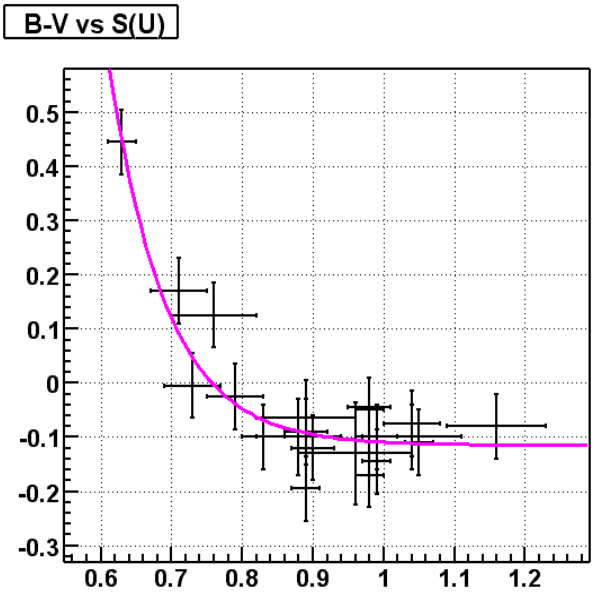

Figure 9. B-V intrinsic color at maximum versus the U-band stretch, fit to an exponential function.

The color at maximum light is not sufficient for determining the color at the

epoch of the NICMOS observations. To estimate the color at other times, we used Rob's U and B lightcurve parameterizations together with the lightcurve maximum color. This approach is valid for a stretch=1 SN by definition. In our case, this is just an approximation based on the assumption that the shape of the uberspectrum is not highly stretch-dependent. To implement this approach, we simply warped the spectrum in the U-band to match the predicted color in each case.

By using the above information and varying the extinction to match the observed NICMOS counts, we estimate $E(B-V)_{host} = 0.075 +- 0.080$. Using the derived extinction and the uberspectrum model, we can convert the U-band lightcurve maximum to the B-band lightcurve maximum, obtaining M(B) = 25.78 +- 0.17 (lightcurve) +- 0.07(extinction).

3. Spectral extinction estimate

Work is in progress to estimate the extinction on the basis of the observed Albinoni spectrum. This spectrum covers both the restframe U and B, and it is therefore hoped that it can help break some of the degeneracy between intrinsic U-B color (or more generally the stretch-dependent behavior of the uberspectrum for s=1.2) and host galaxy extinction. This is the last outstanding piece of analysis needed to complete preparing Albinoni for cosmological measurements. This work is also required to compare the spectrum of Albinoni with that of nearby SNe Ia.

5. Updated cosmology

In preparation for adding Albinoni to the existing SCP cosmology fits, we have reproduced the cosmological results (fits 3 and 6) from the Knop '03 paper using the same fitter [19]. All the numbers were reproduced exactly except the error on α for fit 6 being 0.28 instead of published value of 0.30. A fit with finer grid did not change the results. We consider the discrepancy to be insignificant, probably due to a typographical error.

Work is in progress to incorporate the Albinoni results into the fitting framework.

SN lensing is a issue to which will also have to be addressed for Albinoni. We have used SNOC simulations [19] to assess the lensing probability distribution function (PDF). This has been parameterized in terms of the depending compact mass fraction along the line of sight (Figures 10 and 11). The available limits on the compact matter indicate $\Omega_{compact} < 0.2$ [21], but much stronger constrainst, $\Omega_{compact} < 0.03$ [22], may soon be available. In the most general sense, a possible way to proceed with a single SN such as Albinoni is to incorporate the lensing PDF into the cosmological fitter as part of the flux error.

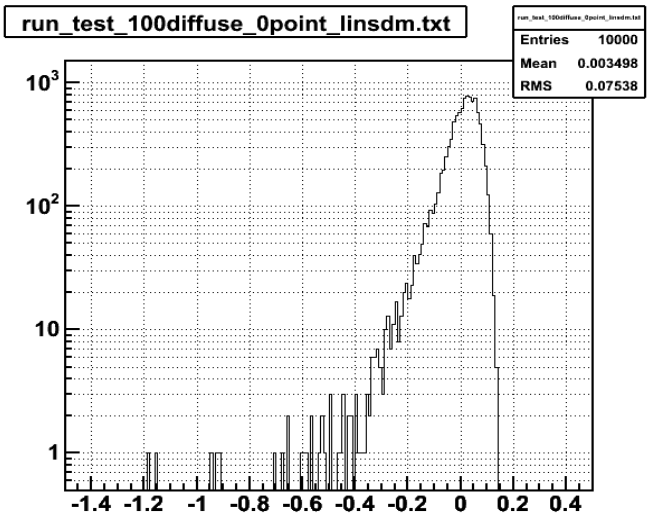

Figure 10. Deviation from the nominal magnitude for redshift 1.2 SN assuming 100% diffuse matter, obtained with SNOC simulation package.

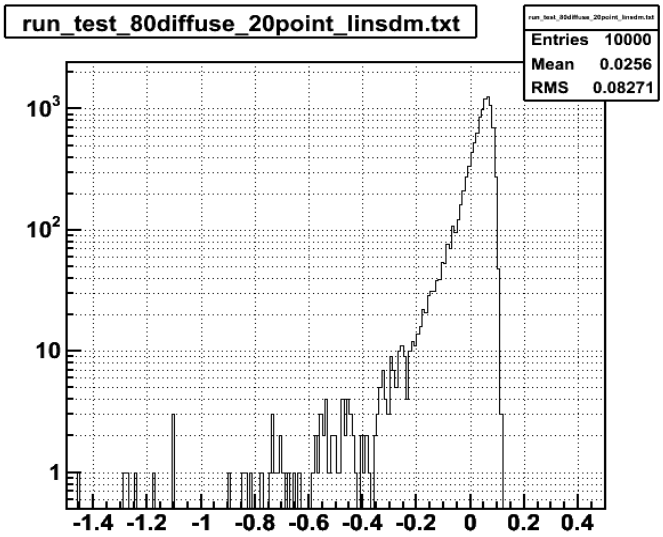

Figure 11. Deviation from the nominal magnitude for redshift 1.2 SN assuming 80% diffuse matter and 20% compact matter, obtained with SNOC simulation package.

6. Conclusions

We have presented the current state of analysis, including the photometric processing, the lightcurve fit and the first extinction estimate.

7. Acknowledgments

We gratefully acknowledge the help of Tom Daley of Earth Sciences Division for help with reading the Exabyte tapes.
We thank Shane Burns for discussions regarding NICMOS data.
We thank Rob Knop for making his software available, introduction and answering numerous questions.
We thank Ralph Bohlin for discussions about the NICMOS photometric calibration.
We thank Alfred Shultz for answering questions regarding NICMOS performance.
We thank Alex Conley for help with loading ground-based images in the SCP database, and for other help.

References

[1] R. Knop and SCP Collaboration, "New Constraints on Ω_M, Ω_Λ, and w from an Independent Set of 11 High-Redshift Supernovae Observed with the Hubble Space Telescope", 2003, ApJ, 598, 102.

[2] G. Aldering, "SN1998eq Analysis Status Report", April 9, 2001.

[3] NICMOS History in Brief, NICMOS Instrument Handbook, http://www.stsci.edu/hst/nicmos/documents/handbooks/DataHandbookv5/ .

[4] R. Knop with S. Deustua, "Data Reduction for the Deepsearch", Version 1.4.0, 2002 June 12.

[5] Rob's instructions for *running* ***ivanlight*** code are available at http://brahms.phy.vanderbilt.edu/deepsearch/scp/ivanlight.html .

[6] The prescription was obtained via private communications with James Schlaerth and Rob Knop.

[7] The code and instructions for Rob's HST software are available at http://brahms.phy.vanderbilt.edu/deepsearch/scp/deepsoft/index.html . The code per se is called ***simplehstltcv***, but one would also need ***Deeplib***, ***SpecLTCV***, and probably ***Rob's Uberspectra and Templates***.

[8] A. S. Fruchter and R. N. Hook, "Drizzle: A Method for the Linear Reconstruction of Undersampled Images", 2002 PASP, 114, 144. The package is available in IRAF as ***stsdas.analysis.dither*** .

[9] The equations, numerical parameters and some text about A. Dolphin's parameterizations can be found at http://www.noao.edu/staff/dolphin/wfpc2_calib/ .

[10] J. Krist and R. Hook, "The Tiny Tim User's Guide", available at http://www.stsci.edu/software/tinytim/ .

[11] S. Malhotra, et al. 2002, "NICMOS Instrument Handbook", Version 5.0, (Baltimore:STScI). See also the advisory about NICMOS anomalies at http://www.stsci.edu/hst/nicmos/performance/anomalies .

[12] V. Fadeyev, G. Aldering, and S. Perlmutter, "Improvements to the NICMOS MULTIACCUM signal processing", the write-up to be completed.

[13] Rene Brun and Fons Rademakers, "*ROOT - An Object Oriented Data Analysis Framework",* Proceedings AIHENP'96 Workshop, Lausanne, Sep. 1996, Nucl. Inst. & Meth. in Phys. Res. A 389 (1997) 81-86. See also http://root.cern.ch/ .

[14] S. Burns, "Albinoni NICMOS Photometry", March 10, 2001.

[15] F.James and M.Roos, "Minuit - a system for function minimization and analysis of the parameter errors and correlations", Comp. Phys. Comm., Volume 10, Issue 6, p. 343. See also F. James, "Minuit, Function Minimization and Error Analysis", CERN long write-up D506, available at http://wwwasdoc.web.cern.ch/wwwasdoc/minuit/minmain.html .

[16] S. Jha, 2002, PhD thesis, Harvard University.

[17] J. Orear, "Least squares when both variables have uncertainties", Am. J. Phys. 50, 10 (1982).

[18] G. Goldhaber etal , 2001, ApJ, 558, 359.

[19] *Omlam* fitter by Rob Knop, http://brahms.phy.vanderbilt.edu/~rknop/scp/omlam/ .

[20] A. Goobar etal, "SNOC: a Monte-Carlo simulation package for high-z supernova observations", ApJ. See also R. Amanullah, E. Mortsell and A. Goobar, "Correcting for lensing bias in the Hubble diagram", A&A 397 819 (2003).

[21] J. Dalcanton etal, "Observational limits on W in stars, brown dwarfs, and stellar remnants from gravitational microlensing", ApJ 424, 550 (1994).

[22] C.C. Wiegert, "Constraining Compact Dark Matter with Quasar Equivalent Widths from the Sloan Digital Sky Survey Early Data Release", astro-ph/0307465.